Steel and Composite Structures, *Vol. 34, No. 6 (2020) 909-927*
DOI: https://doi.org/10.12989/scs.2020.34.6.909

Partially encased composite columns using fiber reinforced concrete: experimental study

Margot F. Pereira[1a], Silvana De Nardin*[1] and Ana L.H.C. El. Debs[2b]

[1]Department of Civil Engineering, Federal University of Sao Carlos, Sao Carlos, Brazil, Rodovia Washington Luís, km 235 - SP-310 São Carlos-SP - CEP 13565-905, Brazil
[2]Department of Structural Engineering, University of São Paulo, São Carlos, Brazil, Avenida Trabalhador Saocarlense 400, Centro, São Carlos-SP - CEP: 13566-590, Brazil

(*Received November 14, 2018, Revised October 31, 2019, Accepted January 4, 2020*)

Abstract. This paper addresses the results of an experimental study involving 10 partially encased composite columns under concentric and eccentric compressive loads. Parameters such as slenderness ratio, ordinary reinforced concrete and fiber reinforced concrete, load eccentricity and bending axis were investigated. The specimens were tested to investigate the effects of replacing the ordinary reinforced concrete by fiber reinforced concrete on the load capacity and behavior of short and slender composite columns. Various characteristics such as load capacity, axial strains behavior, stiffness, strains on steel and concrete and failure mode are discussed. The main conclusions that may be drawn from all the test results is that the behavior and ultimate load are rather sensitive to the slenderness of the columns and to the eccentricity of loading, specially the bending axis. Experimental results also indicate that replacing the ordinary reinforced concrete by steel fiber reinforced concrete has no considerable effects on the load capacity and behavior of the short and slender columns and the proposed replacement presented very good results.

Keywords: partially encased composite columns; steel-concrete composite columns; experimental analysis; steel fiber reinforced concrete; concentric load; eccentric load

1. Introduction

Partially encased composite (PEC) columns are structural elements made with H-shaped steel sections where the space between the flanges and the web are filled up with concrete; steel and concrete working together. This type of composite column is commonly used in modern construction owing to their high strength and the possibility of reducing the construction time, taking advantage of prefabrication and simple installation of formwork. However, according to the main standard codes for these columns, such as ABNT NBR 8800 (2008) and Eurocode 4 (2004), a minimum longitudinal and transversal reinforcement should be provided to prevent cracking and splitting of concrete and it requires intensive labor and difficulties in construction. This requirement leads to a fabrication process involving the laborious task that is the anchoring of the reinforcements to the steel profile. Several experimental and analytical studieshad been carried out on PEC columns. The influence of the concrete strength on the behavior of PEC columns was investigated and, as expected, the ultimate capacity of the columns was increased with the increase of the concrete strength (Hunaiti and Fattah 1994). However, the columns with lower strength concrete presented greater ductility and the cracks appear only for high levels of loading.

The use of non-compact steel components made with three plate built-up steel shape in partially encased columns can be an interesting alternative to achieve overall cost reductions. In this new composite column, the concrete resists a larger portion of the vertical loads while the steel section is responsible for supporting the construction loads and a small part of the total load (Vincent 2000). However, the use of thin steel plates with width-to-thickness ratio that exceeds the standard limits leads to the local buckling of the flanges. The use of transverse links welded at regular spacing along the tips of the flanges have been an alternative investigated by some researchers to increase the local buckling resistance and provide minimum confinement (Vincent 2000, Tremblay *et al*. 2000, Chicoine *et al*. 2002, Chicoine *et al*. 2003, Oh *et al*. 2006). In this case, the failure of the short composite columns occurs by a combination of local buckling of the steel flanges between the links and crushing of the concrete, while the slender columns fail by global flexural buckling combined with local buckling of the steel flanges and crushing of the concrete (Tremblay *et al*. 2000, Chicoine *et al*. 2002, Oh *et al*. 2006). Based on experimental results, some researchers suggest the links can be spaced by half the depth avoiding that the local buckling of the flanges that occurs before the

*Corresponding author, Adjunt Professor
E-mail: snardin@ufscar.br
[a]Professor, Ph.D.
E-mail: margot@ufscar.br
[b]Associate Professor, Ph.D.
E-mail: analucia@sc.usp.br

http://www.techno-press.org/?journal=scs&subpage=6
ISSN: 1229-9367 (Print), 1598-6233 (Online)

peak load (Chicoine *et al*. 2002). A formula for predicting the load capacity of composite columns under concentric loads accounting for the local flanges' buckling and the concrete strength was proposed for design applications (Chicoine *et al.* 2002 and Oh *et al*. 2006). The long-term loading as shrinkage and creep of the concrete had no significant effect on the failure mode and ultimate capacity for this type of composite column (Chicoine *et al.* 2003). The influence of the concrete strength on the load capacity and behavior of the new partially encased column was investigated and the results showed the axial capacity was greatly increased when the normal concrete with 30 MPa strength was replaced by high strength concrete (60 MPa) (Begum and Driver 2013). As reported in the literature (Vincent 2000, Tremblay *et al*. 2000, Chicoine *et al.* 2002, Oh et al. 2006, Chicoine et al. 2003, Begum and Driver 2013, Chen *et al*. 2010, Wang *et al*. 2019), the local buckling of the flanges was taken into account by the use of an effective width which is a function of width-to-thickness ratio and link spacing. This effective width is applied in the equations to predict the axial capacity of the partially encased columns (Tremblay *et al.* 2000, Chicoine *et al.* 2002). Local and post-local buckling behavior of the partially encased columns made with non-compact steel component and reinforced by transverse links was investigated considering the residual stresses of steel (Song and Wang 2016).

Some researchers evaluated the influence of slenderness on partially encased composite columns. For example, Gramblička and Matiasko (2009) studied the influence of the slenderness ratio on PEC columns with high strength concrete under eccentric loading. Tests were carried out on pin-ended columns with slenderness ratios of 0.58 and 0.78. Reduction of 14% in the peak load of the PEC columns was recorded when the slenderness ratio was increased by 35%. In addition, the influence of the slenderness ratio on the load capacity increases with the increase of the concrete strength (Gramblička and Matiasko 2016). Begum *et al.* 2015 also evaluated column slenderness ratio (L/d), among others, in a parametric study on eccentrically loaded columns conducted using finite element tools. Among the important findings, the authors highlight that the ductility of a normal strength concrete columns is reduced as the column slenderness ratio increases. However, for high strength concrete PEC, the level of brittleness at failure is not significantly modified by column slenderness ratio.

Recent works focused on different types of PEC columns, as octagonal partially encased composite columns under axial and torsion loading. (Ebadi Jamkhaneh and Kafi 2017) and fire behaviour of PEC columns embedded on walls (Rocha *et al*. 2018). Wang *et al.* (2019) conducted a study about design recommendations of eccentrically loaded PEC columns and results revealed that the fully plastic assumption could be unconservative in some cases. The use of recycled concrete aggregate (RCA) in concrete of the partially encased composite columns was investigated by Wu *et al*. (2019) and the results showed that the composite columns are a new interesting option for reusing old concrete. Other researchers attempted to improve structural performance of composite elements by using high strength materials. For example, Lai *et al*. (2019) investigated the structural behaviour of composite columns made of high strength steel (300 to 780 MPa) and high strength concrete (150 to 190 MPa).

The use of fiber reinforced concrete (FRC) has many advantages including elimination of microcracks at early stages of concrete, lower permeability, improved resistance to explosive spalling in case of a severe fire and improved mechanical properties at the post-cracking stage. In the last decade there was a series of studies concerning the use of steel fiber reinforced concrete in composite columns, however, most of them involving concrete filled steel tube composite columns (Hatzigeorgiou and Beskos 2005, Ellobody *et al.* 2018a, Ellobody *et al*. 2018b, Lu *et al*. 2017, Lu *et al*. 2018) or reinforced concrete columns (Tokgoz and Dundar 2010, Tokgoz 2015). However, this specific type of composite column have a peculiarity: the steel tube confines the concrete core. In contrast to the filled columns, in the partially encased columns the confinement of the concrete is not so effective. The effect of fibers on the structural behaviour of other composite elements, such as composite deck slabs, was studied (Altoubat *et al.* 2015). In this case, the results show that the fibers induced multiple cracking improving the ductility of composite deck slabs.

Authors such as Prickett and Driver (2006) and Ellobody and Ghazy (2013) evaluated the influence of the concrete strength and the steel fibers' addition on the behavior of partially encased composite columns. Prickett and Driver (2006) conducted experimental tests in partially encased composite columns made of thin plates and stiffened flanges with transversal links. According to their results, the columns with usual compressive strength concretes have a more ductile failure mode than those with high strength concrete. The addition of steel fibers to the high strength concrete and the use of closer-spaced transversal links increase the deformation capacity and produces a less brittle failure mode (Prickett and Driver 2006).

Almost all studies found in the literature combine the steel fiber reinforced concrete with longitudinal and transverse steel bars. In order to improve the structural behavior, simplify the constructive procedures, and develop a more practical and efficient PEC columns, some researchers studied the influence of replacing the conventional longitudinal and transverse steel bars by welded wire mesh in PEC columns under concentric loads (Pereira *et al.* 2016). A previous study showed that the effect of the type of reinforcement on the load capacity, stiffness and post-peak behavior was not significant and the welded wire mesh can be used to replace the conventional steel bars simplifying the fabrication procedure (Pereira *et al.* 2016). However, the authors suggest that these results must be confirmed by new experimental programs for more details on the proposed replacement.

An important aspect in the constructive procedure of partially encased composite columns is the obligation to use longitudinal and transverse reinforcement attached to the web of the steel profile. The positioning of these reinforcements makes construction procedures difficult due to the need to cut, bend and attach to the steel profile.

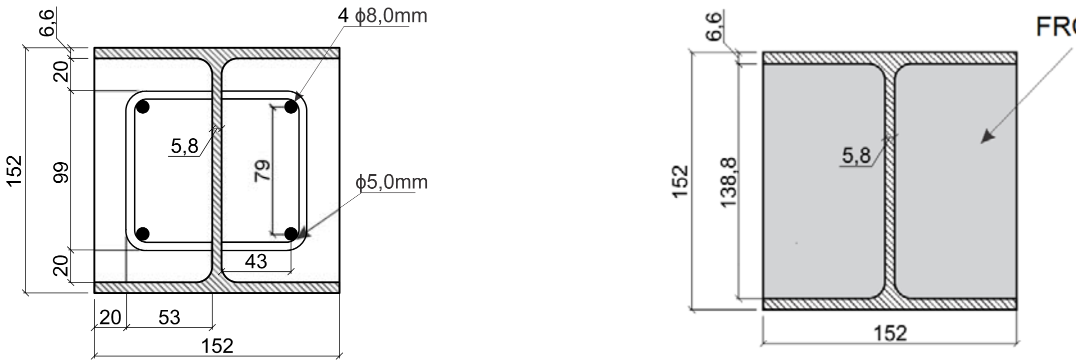

(a) Conventional reinforcements (b) FRC

Fig. 1 Specimens configuration

(a) x eccentricity specimens (b) y eccentricity specimens

Fig. 2 Eccentricity of the axial load

Additionally, it can impede the concrete casting. Therefore, replacing reinforcement with fiber-reinforced concrete can bring significant advantages to construction advantages.

Although the use of fiber reinforced concrete is very common in structural elements there are no studies were the focus was investigate the effects of replacing the steel bars by fiber reinforced concrete in partially encased columns under eccentric loads. In this context, the main objective of the present study is to investigate experimentally the behavior and load capacity of partially encased composite columns under concentric and eccentric axial loads with conventional reinforcement and fiber reinforced concrete. A series of ten tests were conducted on short and long pin-ended composite columns. The attractive advantage of the fiber reinforced concrete (FRC) over reinforced concrete with steel bars is its easy handling with minimal time and labor.

2. Experimental program

2.1 Geometric properties of tested specimens

Ten partially encased composite columns having similar cross section and made with concrete reinforced with conventional reinforcements or with fiber reinforced concrete (FRC) were tested in this study (Fig. 1).

The tests are divided into two series as a function of the column length and of the eccentricity axes. Series 1 corresponds to six short columns (S-RC-0, S-FRC-0, S-RC-25y, S-FRC-25y, S-RC-25x and S-FRC-25x) subjected to concentric or eccentric compression loading with eccentricity in one of the principal axes (Fig. 2). In Series 2, four relatively long columns (L-RC-0, L-FRC-0, L-RC-25x and L-FRC-25x) were subjected to axial compression or eccentric compression with eccentricity just in the x axis. All specimens of series 1 and 2 had a cross section of 152 x 152 mm and heights of 600 mm and 2,000 mm respectively. For each specimen of both series, the same W152 x 22.5 steel profile was used for the composite cross section. All the tested specimens were made by filling the space between the flanges of the steel profile with reinforced concrete. Specimens of series 1 had ordinary reinforcement configuration (Fig. 1(a)) composed by four longitudinal steel bars with 8 mm diameter and transverse reinforcements achieved using stirrups with a diameter of 6.3 mm. The stirrups were placed at the intervals of 90 mm and 100 mm for Series 1 and Series 2, respectively. At both ends of specimens, the spacing of stirrups was reduced to prevent local failure. In the specimens filled with FRC (Fig. 1b), stirrups were used only 300 mm from the end to prevent local failure. In all specimens with ordinary reinforced concrete, the stirrups were welded to the web of the steel profiles. Table 1 summarized the test specimens and the tested parameters.

Table 1 Characteristics of tested specimens

Series	Specimen	Axial load	e_i^* (mm)	Length (mm)	Concrete	Reinforcement	f_c (MPa)
1	S-RC-0	CG*	0	600	Plain	Ordinary	36.7
	S-FRC-0	CG	0	600	FRC	-	34.8
	S-RC-25y	e_y	25	600	Plain	Ordinary	36.7
	S-FRC-25y	e_y	25	600	FRC	-	34.8
	S-RC-25x	e_x	25	600	Plain	Ordinary	36.7
	S-FRC-25x	e_x	25	600	FRC	-	34.8
2	L-RC-0	CG	0	2000	Plain	Ordinary	36.7
	L-FRC-0	CG	0	2000	FRC	-	34.8
	L-RC-25x	e_x	25	2000	Plain	Ordinary	36.7
	L-FRC-25x	e_x	25	2000	FRC	-	34.8

*CG: center of geometry; e_i: initial load eccentricity; f_c: compressive strength of concrete

Fig. 3 Detail of knife bearings

2.2 Mechanical properties of materials

Specimens filled with ordinary reinforced concrete used a mixed with a ratio of cement, sand, aggregate of maximum size 9,5 mm, and water as 1, 2.42, 2.58, and 0.68, respectively. The estimated consumption of cement was 365 kg/m³. For the FRC, the same mixture of plain concrete was used with addition of two types of steel fibers with average lengths of 25 mm and 33 mm. The two lengths of fibers were mixed and added at the volume fractions of 1.5% of the concrete volume. This amount was chosen because there are enough fibers to influence the ductility of the concrete, but not so many that make workability difficult.

The material properties of steel and concrete were obtained from respective tensile and compressive tests. The properties of steel profiles were determined by tensile coupon tests, according to ASTM A370 (2005), and the average static yield stress was determined as 385 MPa. In both, plain and FR concrete, the investigated mechanical properties include the compressive strength and the elasticity modulus. All specimens of columns with plain concrete were filled in the same day using concrete provided by a ready-mix factory.

Three 100 x 200 mm cylinders were cast from each mixture of concrete (plain and FR concrete) and cured under the same environmental conditions as the specimens. The compressive strengths of those standard cylinders were obtained the same day of the tests. Concrete strength at testing was36.7 MPa and 34.8 MPa, for plain and FR concrete, respectively. Additionally, the modulus of elasticity of concrete was determined at testing to be 26 GPa and 27 GPa, for plain and FR concrete, respectively. Table 1 presents the average values of the mechanical properties of the materials used in the tested specimens. The properties of steel bars were also determined by tensile tests and the average static yield stress was determined as 680 MPa and 524 MPa, for bars with 5 mm diameter and 8 mm diameter, respectively.

2.3 Test setup and loading procedure

The specimens were loaded using a servo-controlled universal testing machine with 2500 kN of nominal capacity. Axial loading with displacement control and at a speed of 0.005 mm/s was applied to the column specimens. All the specimens were pin-ended at both ends using knife bearings (Fig. 3). The load was introduced simultaneously to the steel and concrete e providing the composite action by load sharing. Therefore, bond resistance between steel profile and concrete is not an important factor in this case.

Specimens under concentric and eccentric loading were tested until failure and the behavior was evaluated. For the specimens under eccentric loading the initial eccentricities

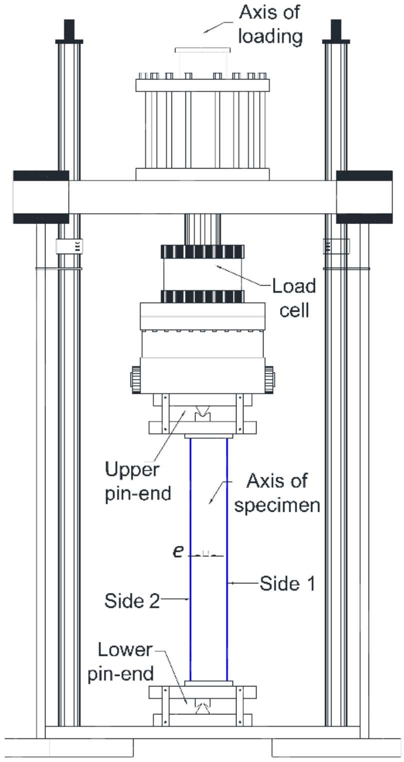

Fig. 4 General layout of test setup: specimens under eccentric loading

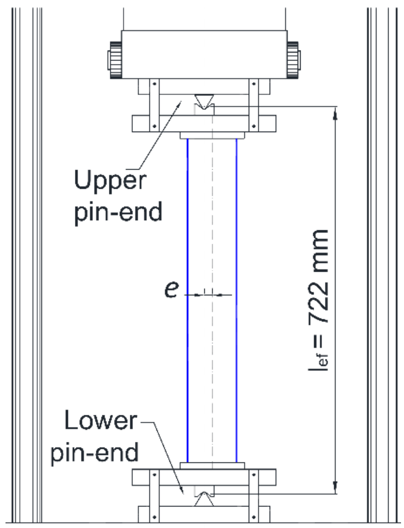

Fig. 5 General layout of test setup for Series 1

were the same and equal to 25 mm at both ends (Fig. 4). The direction of the eccentricity on the major or minor axes depends on the specimen (see Table 1).

The general layout of the test-setup used for both series are shown in Figs. 5 and 6, respectively for Series 1 and Series 2.

2.4 Instrumentation and measurement system

The specimens were instrumented with strain gauges and displacement transducers. The strain gauges were located on the steel profile (flanges and web) and on the concrete in the mid-height region of the specimens. The location of the strain gauges in the cross section was

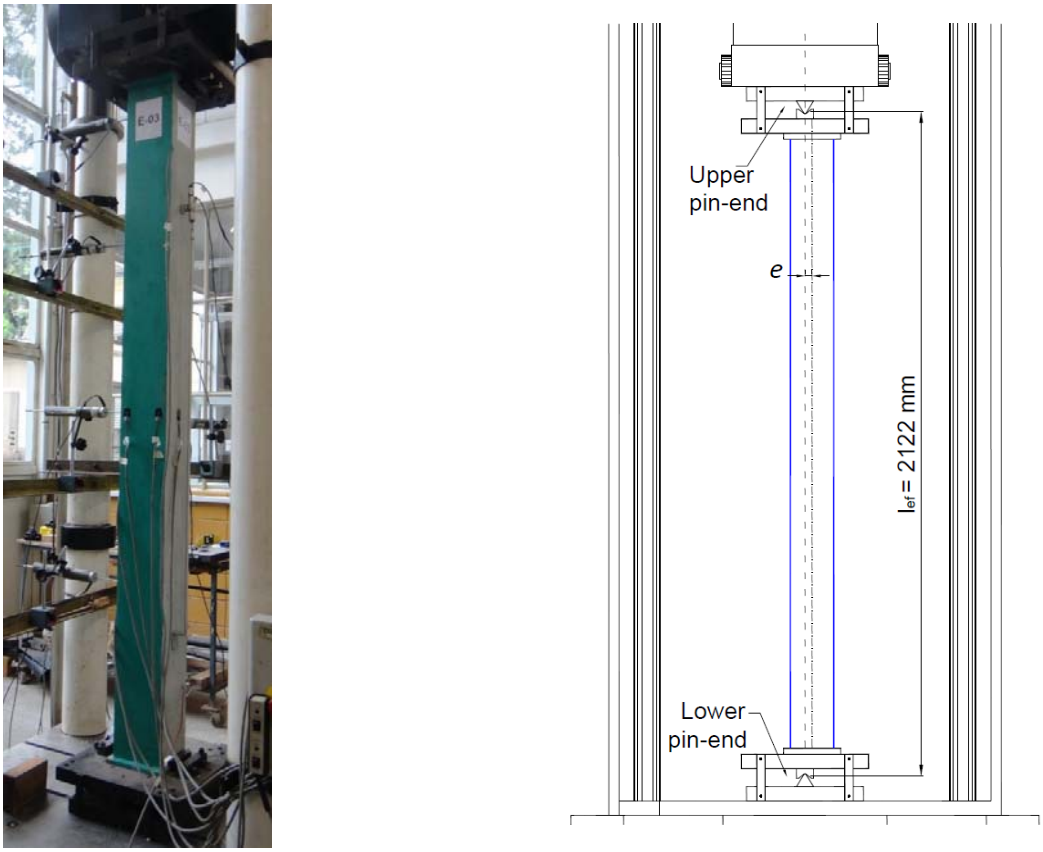

Fig. 6 General layout of test setup for Series 2

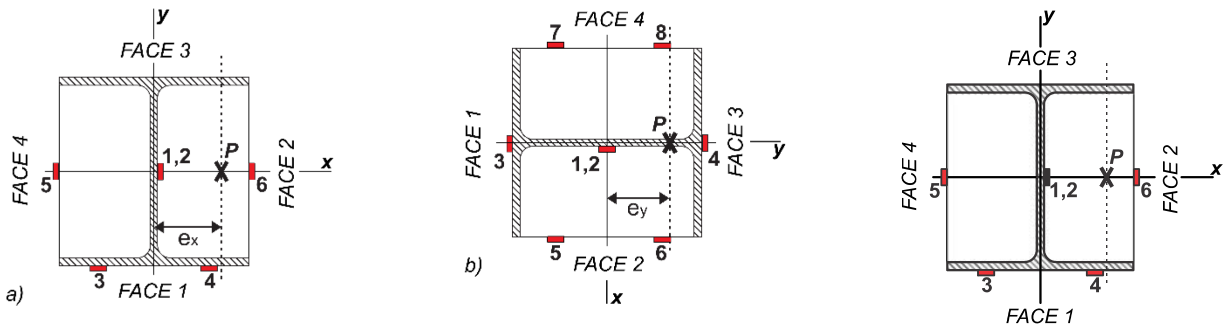

(a) Series 1 - x eccentricity (b) Series 1 - y eccentricity (c) Series 2 - x eccentricity

Fig. 7 Location of strain gauges

defined according to the direction of the eccentricity as shown in Fig. 7.

Axial shortening of the Series 1 specimens was measured using two displacement transducers (1 and 2) installed in the column's faces (Fig. 8). The displacement transducers 3, 4 and 5 measured the lateral deflection in both principal directions. Fig. 8 presents the location of the displacement transducers according to the load position in each specimen.

Due to the longer length of the Series 2 specimens, the axial shortening in these specimens was evaluated using three displacement transducers (1, 2 and 3) as shown in Fig. 9. The displacement transducers 4 to 8 were used to record the lateral deflection in both principal directions (Fig. 9).

3. Results

3.1 Experimental observations and failure loads

3.1.1 Series 1

A general view of the specimens with 600 mm length after failure is shown in Fig. 10. Specimens S-RC-25y and S-FRC-25y (eccentricity about y axis) failed by concrete crushing together with local buckling at the same location, both phenomena on the more compressed face. Similar behavior was observed in specimens with eccentricity about x axis (S-RC-25x and S-FRC-25x) where the failure also occurred by crushing of concrete on more compressed face and cracking of the concrete on the less compressed face

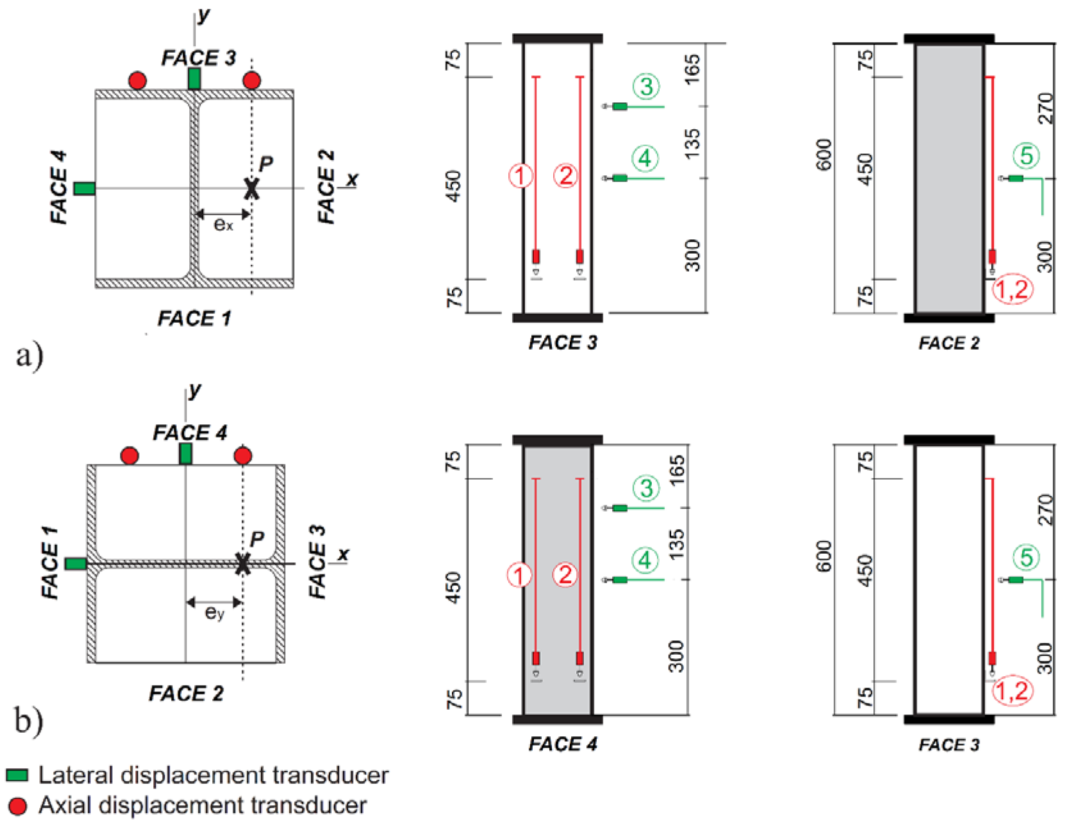

Fig. 8 Displacement transducers in specimens of the Series 1: a) axis x eccentricity; b) axis y eccentricity

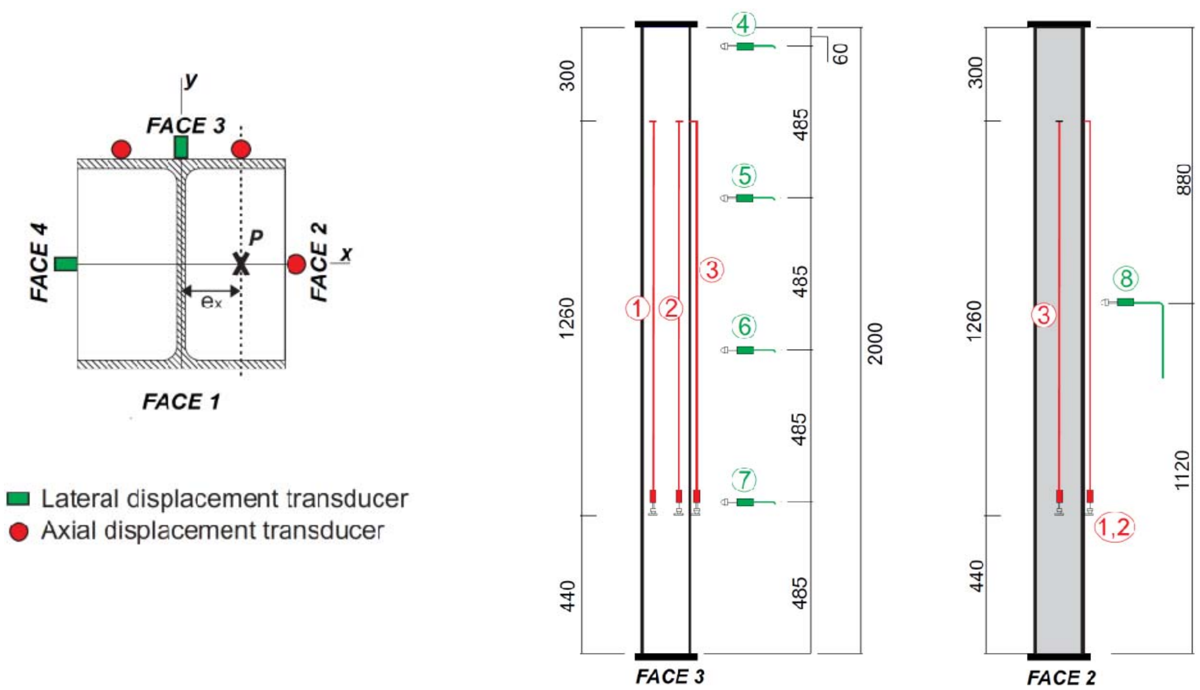

Fig. 9 Mesh grid of topographic model

except that the local buckling was observed only on specimen S-RC-25x. However, the failure was more brittle and sudden than the failure observed on specimens with eccentricity about x axis. Therefore, the bending axis had influence on the behavior after the peak load.

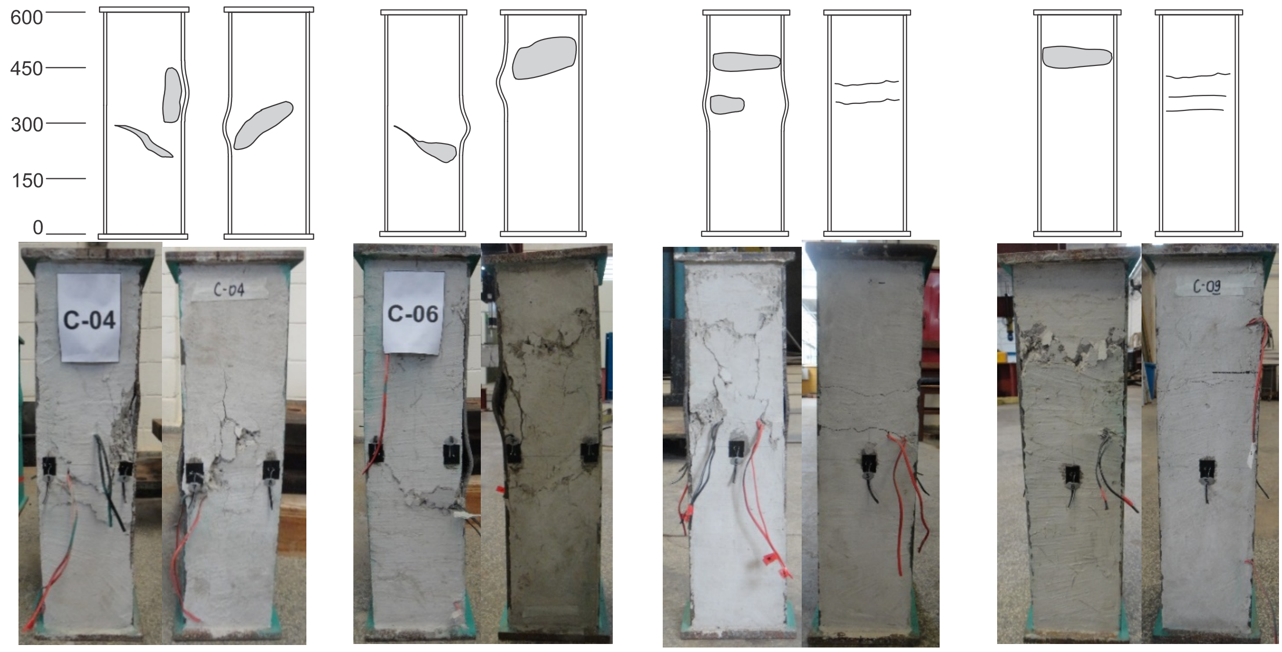

Face 2 Face 4 Face 2 Face 4 Face 2 Face 4 Face 2 Face 4

(a) S-RC-25y (b) S-FRC-25y (c) S-RC-25x (d) S-FRC-25x

Fig. 10 Final configuration of Series 1 specimens

Table 2 Summary of test results

Specimen	f_c	$e_{x.i}$	$e_{y,i}$	δ_x^*	δ_y^*	P_{exp}	M_x	M_y
	(MPa)	(mm)	(mm)	(mm)	(mm)	(kN)	(kN.cm)	(kN.cm)
S-RC-0	36.7	0	0	-0.863	-0.930	1803.96	697	709
S-FRC-0	34.8	0	0	-0.642	-1.821	1648.91	601	795
S-RC-25y	36.7	0	25	-2.398	-0.330	1360.79	4137	-
S-FRC-25y	34.8	0	25	-2.235	-0.294	1336.30	4040	-
S-RC-25x	36.7	25	0	0.018	-3.289	1189.03	-	3720
S-FRC-25x	34.8	25	0	0.514	-2.316	1178.12	-	3572
L-RC-0	36.7	0	0	-0.771	-5.99	1604.28	605	1442
L-FRC-0	34.8	0	0	0.541	3.46	1717.36	608	1109
L-RC-25x	36.7	0	25	0.092	-18.31	913.27	-	4229
L-FRC-25x	34.8	0	25	0.312	-15.48	823.31	-	3580

*Lateral deflection at ultimate load; $M = F \cdot (e_i + e_a + \delta)$

The experimental values of ultimate load (P_{exp}) and bending moment resistance for concentrically and eccentrically loaded specimens (M_x or M_y) are presented in Table 2. The values of bending moment were calculated by multiplying the experimental ultimate load by the total mid-height lateral deflection at ultimate load that is the sum of initial load eccentricity (e_{xi} or e_{yi}) and the mid-height lateral deflection at ultimate load (δ_x or δ_y). Although the specimens S-RC-0 and S-FRC-0 were subjected to concentric loading, the difficulty of specimen centralization and imperfections due to the fabrication process causes an accidental eccentricity in all the tested columns.

The experimental ultimate load measured for the FR concrete specimen (S-FRC-0) was approximately 10% less than the value measured for the specimen with plain concrete and conventional reinforcement (S-RC-0). This reduction can be caused by two factors: contribution of longitudinal reinforcement and the lower FRC strength (5% lower than plain concrete strength). The introduction of an initial load eccentricity in the application of loads reduces the ultimate force about 24% and 19% respectively for conventional reinforcement and FRC specimens. Similar behavior was observed for eccentrically loaded columns with FRC and plain concrete.

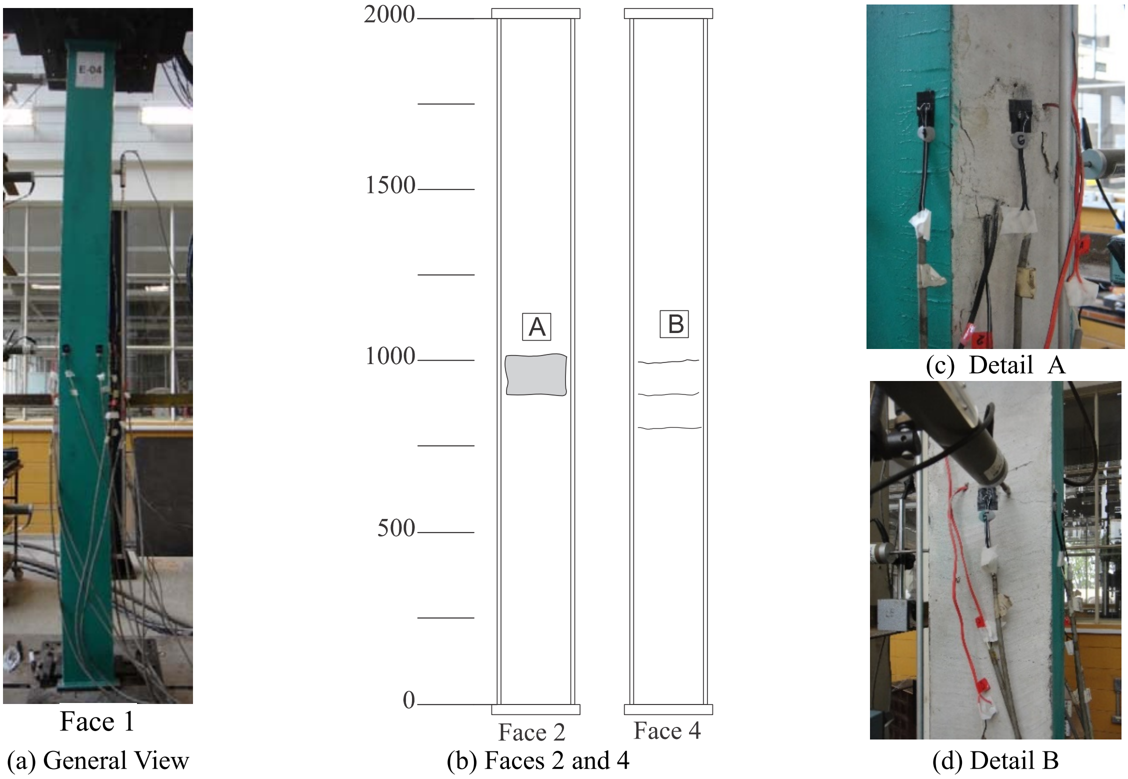

Fig. 11 Final configuration of specimen L-RC-25x

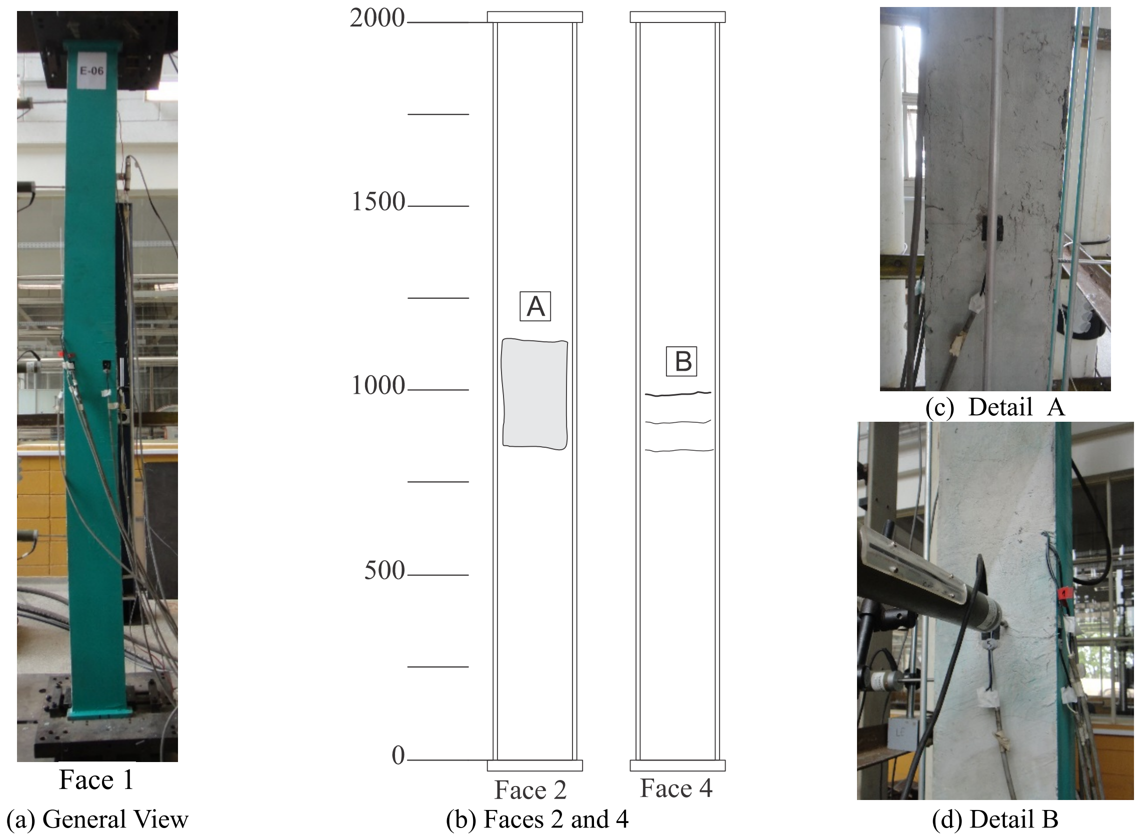

Fig. 12 Final configuration of specimen L-FRC-25x

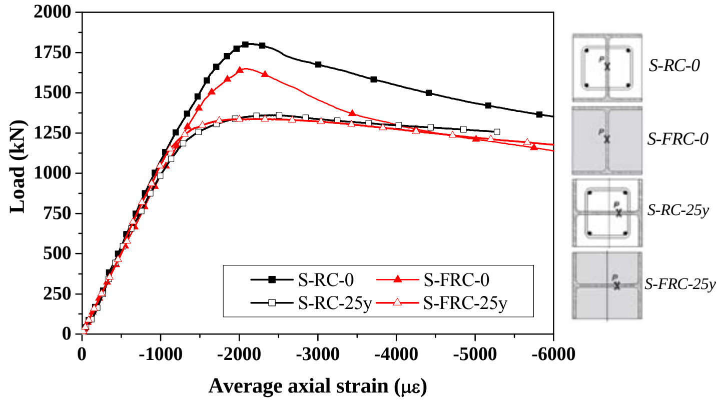

(a) Load vs. Average axial strain

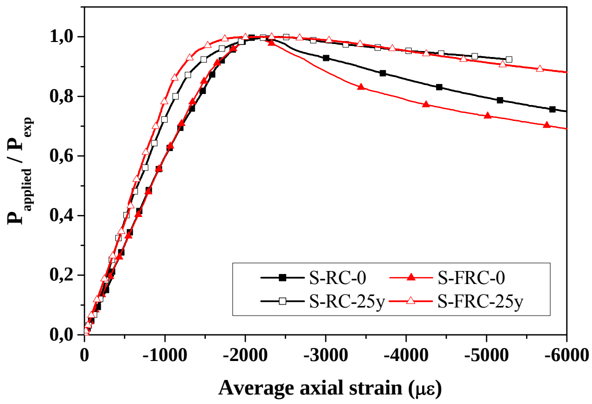

(b) $P_{applied}/P_{exp}$ vs. Average axial strain

Fig. 13 Load vs. average axial strain curves of specimens S-RC-0, S-FRC-0, S-RC-25y and S-FRC-25y

3.1.2 Series 2

A general view of the specimens with 2000 mm length, specimens L-RC-25x and L-FRC-25x, after failure is shown in Figs. 11 and 12, respectively. The eccentrically loaded specimens presented a more ductile response than the concentrically loaded specimens. Crushing of the concrete (Figs. 12(b) and 12(c)) was concentrated in small portions in all specimens of this series, especially for the specimen L-FRC-25x (Fig. 12(c)); tensile cracks were observed in face 2 (Fig. 12(d)). The visible single curvature bending was observed in all tested specimens.

The experimental values of ultimate load (P_{exp}) and bending moment resistance for concentrically and eccentrically loaded columns (M_x or M_y) are presented in Table 2. Comparing the specimens with 2000 mm length under concentric load (L-RC-0 and L-FRC-0) the specimen with ordinary reinforced concrete (L-RC-0) presented ultimate load approximately 7% lower than that obtained for specimen L-FRC-0. This fact was unexpected because the conventional longitudinal reinforcement contributes to resistant capacity, being the predicted ultimate load for L-RC-0 greater than predicted ultimate load for L-FRC-0. Moreover, the concrete strength in specimen L-RC-0 was slightly higher than the specimen L-FRC-0, 36.7 MPa and 34.8 MPa, respectively, and this also contributes to increase the ultimate load. This result probably was caused by a higher accidental eccentricity due to imperfections in the shape or on the positioning of the specimen L-RC-0, resulting in a lower ultimate load. On the other hand, the ultimate load of the eccentrically loaded specimens was the expected value, ie, the specimen L-FRC-25x (specimen with FR concrete) presents a lower resistant capacity than the specimen with plain concrete and conventional reinforcement (specimen L-RC-25x). The ultimate values were 823.31 kN and 913.27 kN respectively for the specimens with FRC and with ordinary reinforced concrete. The influence of the fibers and eccentricity of load is detailed in the item 3.4.

The introduction of initial load eccentricity in the load application reduces the measured values of the ultimate load about 25% for conventionally reinforced specimens (specimens L-RC-0 and L-RC-25x) and 52% FR concrete specimens (specimens L-FRC-0 and L-FRC-25x).

3.2 Load vs. Strains behavior

3.2.1 Series 1

Fig. 13 presents the axial load with respect to the average axial strain for the specimens of Series 1, with 600 mm length (specimens S-RC-0, S-FRC-0, S-RC-25y and S-FRC-25y). The average axial strain in Fig. 13 and Fig. 14 corresponds to the average shortening of the columns measured by the displacement transducers 1 and 2 divided

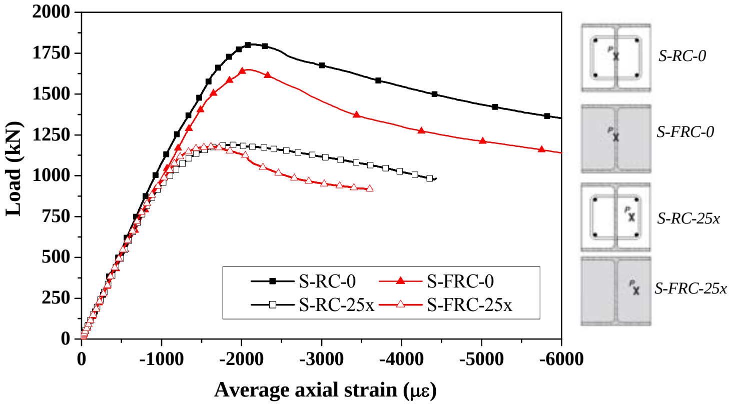

(a) Load vs. Average axial strain

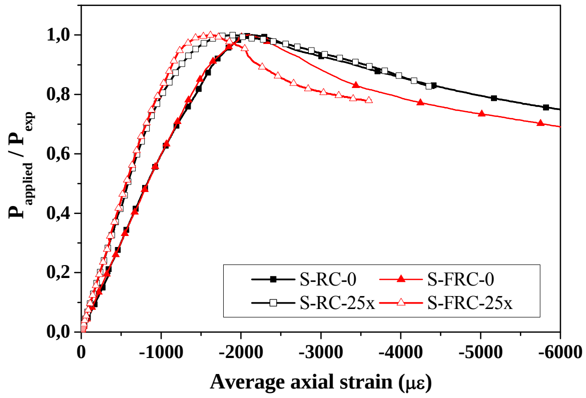

(b) $P_{applied}/P_{exp}$ vs. Average axial strain

Fig. 14 Load vs. average axial strain curves of specimens S-RC-0, S-FRC-0, S-RC-25x and S-FRC-25x

by the length between their attachment points on the column (450 mm). The behavior curves of the Series 1 specimens indicates a ductile response, with strains at peak load reaching almost 2000 με and similar linear behavior up to a 750 kN (Fig. 13(a)). After reaching the peak load, the concentrically loaded specimens (S-RC-0, S-FRC-0) exhibited a gradual and considerable decline in the post-peak branch while the specimens S-RC-25y and S-FRC-25y exhibited a softer post-peak response, maintaining a higher load capacity (Fig. 13(b)). Specimens S-RC-0 and S-FRC-0, both under concentric load, and respectively with ordinary reinforced concrete or FR concrete presented the same behavior on the pre-peak branch (Fig. 13(b)). Moreover, the response of both specimens under concentric load was almost linear and identical until approximately 0.8 of the peak load. For these specimens, a response indicates the insignificant influence of the type of concrete on the structural behavior until the peak-load. In the post-peak branch, the specimen with ordinary reinforced concrete (S-RC-0) presented a higher residual load capacity than the specimen with FR concrete (S-RC-0). The small differences between specimens S-RC-0 and S-FRC-0 in the post-peak branch suggest that the concrete type (ordinary reinforced concrete or FR concrete) can affect the behavior after the peak and deformation capacity.

The pre-peak response of the specimens with 600 mm length under concentrically load (S-RC-0 and S-FRC-0) and with eccentricity about y axis (S-RC-25y and S-FRC-25y) indicates there was no significant influence by the type of concrete (ordinary reinforced concrete or FR concrete) on the structural behavior.

The response of the specimens under concentric load (specimens S-RC-0 and S-FRC-0) and with eccentricity about x axis (specimens S-RC-25x and S-FRC-25x) is compared in Fig. 14 using the Axial load vs. Average axial strain Curves (Fig. 14(a)) and the ratio between the Applied load ($P_{applied}$) and the Ultimate load (P_{exp}) in each tested specimen. All specimens presented a linear behavior until 0.75 peak load (Fig. 14(b)). The behavior of the specimens S-RC-0, S-FRC-0, S-RC-25x and S-FRC-25x in the pre-peak branch was similar until almost 750 kN (Fig. 14(a)). As previously mentioned, specimens with smaller length (S-RC-0 and S-FRC-0) presented identical behavior until the peak load. Comparing the post-peak branch behavior of specimens under eccentric load it can be observed that the load drop was more sudden for the specimen S-FRC-25x than for the S-RC-25x specimen; however, the residual capacity of specimen with fiber reinforcement (S-FRC-25x) was lower than the specimen with conventional reinforced concrete (S-RC-25x). The strains at peak load were 1,850με and 1,600με respectively for the specimens S-RC-25x and S-FRC-25x. Those values are lower than the ones observed for the specimens with no initial eccentricity (concentrically loaded). The response of specimens under load applied on

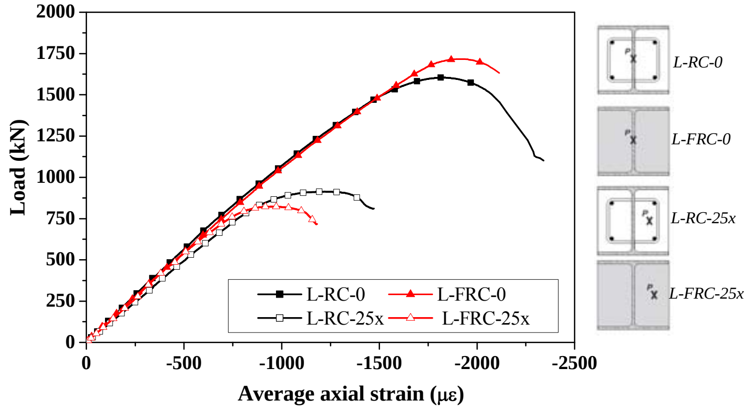

(a) Load vs. Average axial strain

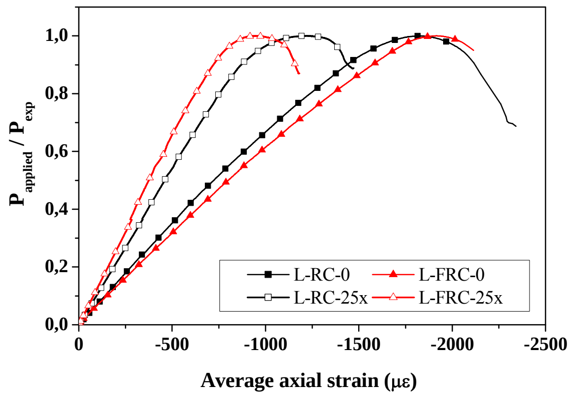

(b) $P_{applied}/P_{exp}$ vs. Average axial strain

Fig. 15 Load vs. average axial strain curves of specimens L-RC-0, L-FRC-0, L-RC-25x and L-FRC-25x

the x axis (S-RC-25x and S-FRC-25x) was identical until the peak load (Fig. 14(b)) indicating no influence of the type of concrete in this branch of loading. The results also indicate that replacing the ordinary reinforced concrete by FRC only influences the post peak response, after the peak load has been reached (Fig. 14(b)).

3.2.2 Series 2

Fig. 15 presents the Axial load vs. the average axial strain of the specimens L-RC-0, L-FRC-0, L-RC-25x and L-FRC-25x. In the same way as the Series 1 specimens, the average axial strain corresponds to the average shortening of the columns divided by the length between displacement transducer's attachment points on the column (in this case, 1260 mm). It can be concluded that the behavior did not vary much from one specimen to another, independently of the reinforcement configuration (reinforced concrete or FR concrete). For the longer specimens under concentric load (L-RC-0 and L-FRC-0), the behavior was linear up to approximately the load corresponding to 70% of the peak load (Fig. 15(b)). Very similar response was recorded for the specimens under eccentric load and their response was linear up to 80% of the peak load. The strains at peak load were 1,828, 1,900, 1,219 and 950 με for specimens L-RC-0, L-FRC-0, L-RC-25x and L-FRC-25x, respectively (Fig. 15(a)). Therefore, the specimens under concentric load (L-RC-0 and L-FRC-0) experienced much higher axial strains than those observed for the specimens under eccentric load (L-RC-25x and L-FRC-25x). In contrast to the observed values in the specimens of the Series 1, the post-peak branch of the longer specimens (Series 2) presented no residual capacity. The load drop of the specimens L-FRC-0, L-RC-25x and L-FRC-25x was so sudden that only a few readings could be taken after the peak load. Among all the specimens under eccentric load, only L- RC-0 presented more readings after the peak load. Furthermore, the post-peak response of the Series 2 specimens presents very abrupt load change and it was not possible to identify the residual capacity for these specimens (Fig. 15). Therefore, the slenderness ratio influenced the post-peak response and the ductility of the tested specimens.

3.3 Strains in the steel profile and concrete

Fig. 16 illustrates the strains developed in the steel profile (3 and 4) and in the concrete (5 and 6) corresponding to the strain gauges 3, 4, 5 and 6 of the specimens S-RC-25y, S-FRC-25y, S-RC-25x and S-FRC-25x. All Series 1 specimens under eccentric load experienced high axial strains in the steel profile confirming the yielding of the steel under compressive stresses. Unlike the other specimens, no local buckling of the compressed flange was observed in the specimen S-FRC-25x after the peak load (Fig. 10). Steel strains reached up to about

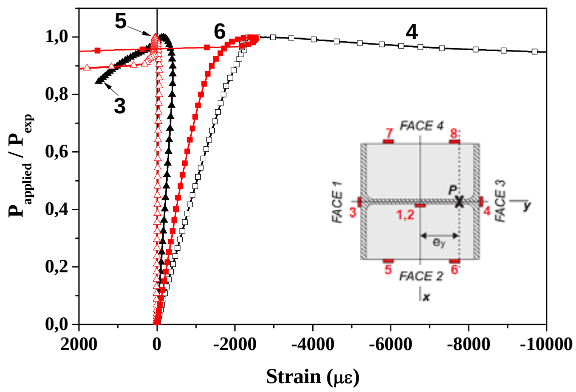

(a) Specimen S-RC-25y

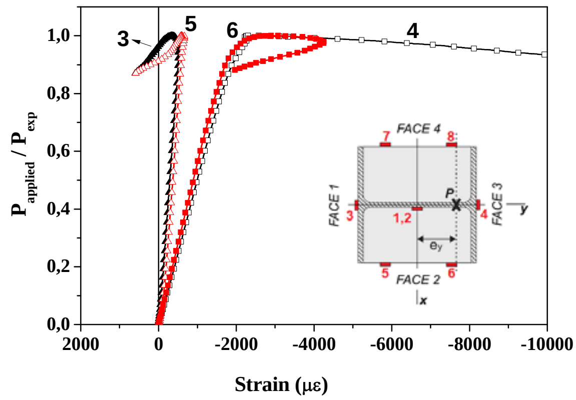

(b) Specimen S-FRC-25y

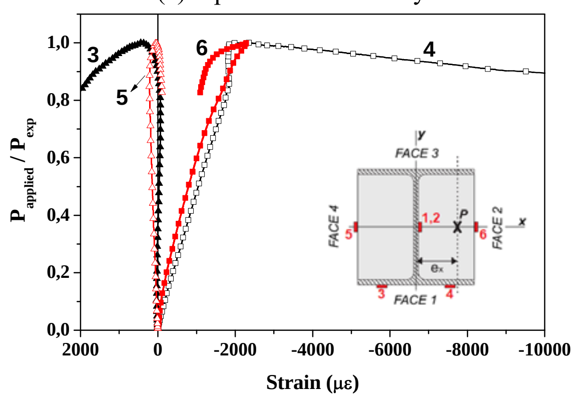

(c) Specimen S-RC-25x

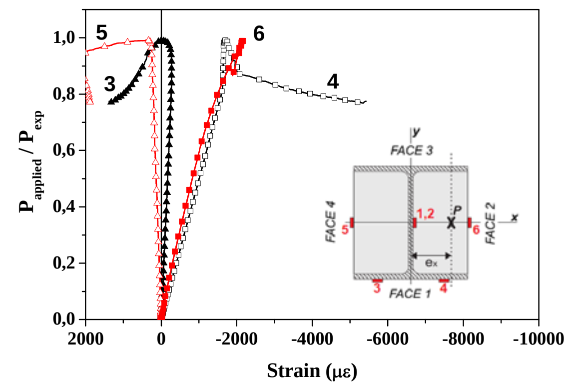

(d) Specimen S-FRC-25x

Fig. 16 Load vs. Strain curves of Series 1 specimens

10,000με and were more pronounced in the compressed flange of the specimens S-RC-25y (Fig. 16(a)) and S-RC-25x (Fig. 16(c)), under eccentricities about y axis and about x axis respectively. Among all the specimens, S-FRC-25y presented strain values close to each other in the steel profile and in the concrete up to 95% of the peak load. The behavior of the strain in the concrete indicates a ductile response of this material (point 6, Fig. 16(b)). Comparing the specimens S-RC-25y and S-FRC-25y, the strain readings indicate the addition of steel fibers increased the strain corresponding to the peak load (Figs. 16(a) and 16(b)). Moreover, the response of the FR concrete (point 6, Fig. 16(b)) exhibited a soft post-peak while maintaining a much higher capacity of deformation. The axial strains in the specimen S-FRC-25x revealed compressive strains in the flange of the steel profile and tensile strains in the concrete between the flanges, indicating that the neutral axis cuts the cross section near to the most compressed face (face 2, Fig. 16(d)).

Comparing the strains in the specimens of Series 1 and 2, the shorter specimens presented higher strains than those recorded in the longer specimens, reaching up to about 6,000 με (Fig. 17). For specimens L-RC-0 and L-FRC-0 of the Series 2, the strain gauges 1, 3 and 4 correspond to the strains in the steel profile and the strain gauges 5 and 6 measured the strains in the concrete. In the case of the longer specimens under concentric load, measurements in the most compressed region of the steel flanges (strain gauge 4) revealed that the strain at peak load was 3,200με and 2,000με for specimens L-RC-0 and L-FRC-0, respectively. These values indicate the yielding of the steel occurred at 95% of the peak load for L-RC-0 (Fig. 17(a)) and only in the post-peak for the specimen L-FRC-0 (Fig. 17(b)). A similar response was showed by the strains recorded in the web of the steel profile (strain gauge 1): the strain at peak load was 2,500με and 1,800με for specimens L-RC-0 and L-FRC-0, respectively. Strain values in the steel and in the concrete are in good agreement with each other, especially on the most compressed face. Due to the sudden load drop in the specimen L-FRC-0, it was not possible to evaluate the post-peak response of this specimen.

The evolution of the strains in the steel profile and in the concrete for the longer specimens eccentrically loaded using ordinary reinforced concrete (L-RC-25x) and FR concrete (L-FRC-25x) is shown in Fig. 17(c) and in Fig. 17(d), respectively. The strains recorded in the most compressed region of the steel flanges presented values greater than that obtained in the web. For both specimens the strain at the peak load was almost 1,000με for the web and ranged from 2,000με to 3,000με in the flanges of the specimens L-RC-25x (Fig. 17(c)) and L-FRC-25x (Fig. 17(d)), respectively. These strain values indicate that flanges of the specimens with 2,000mm length under eccentric load reached the yielding. Although the strain gauges 4 (steel) and 6 (concrete) are not positioned in exactly the same place, the strain gauge readings in the extreme compressive face of the specimens L-RC-25x and L-FRC-25x were close to each other indicating the steel

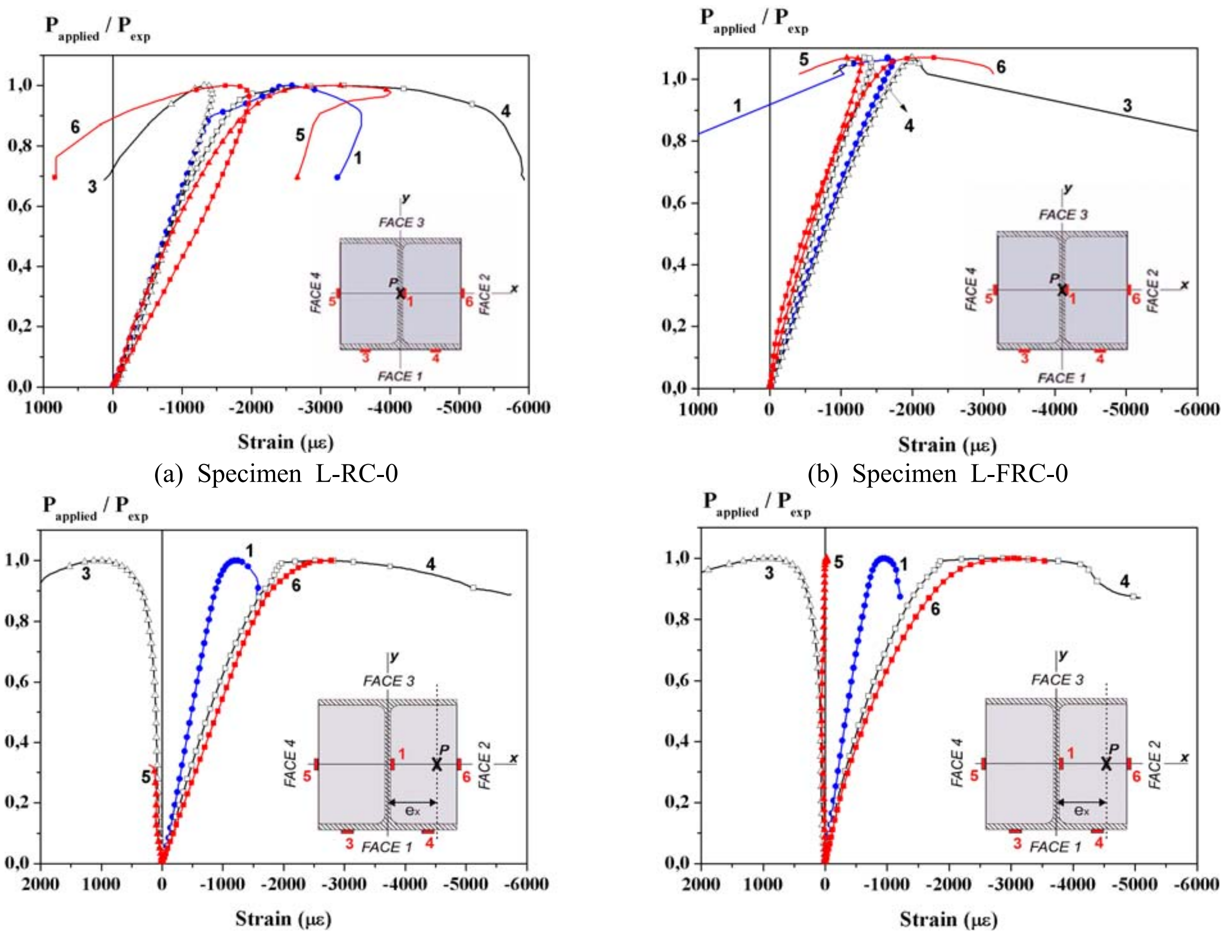

(a) Specimen L-RC-0

(b) Specimen L-FRC-0

(c) Specimen L-RC-25x

(d) Specimen L-FRC-25x

Fig. 17 Load vs. Strain curves of Series 2 specimens

deforms at the same ratio as the concrete. In contrast to the most compressed face, in the least compressed face the behaviors of steel and concrete were very similar until a certain load level and after this the responses of steel and concrete diverge from each another. In the L-RC-25x specimen, at 30% of peak load, a crack appeared at the concrete near the point where the strain gauge 5 was fixed, damaging it and its readings. Although the strain gauge 5 of the specimen E-06 was undamaged, very small strains were recorded until the end of the test. Moreover, it can be observed that the strain response in the steel (point 4) and in the concrete (point 6) presented almost identical values until 50% of peak load and from that point there was an increase in the strains of the steel while in the concrete the strains were almost zero (Fig. 17(d)). This response of the concrete strains in the Specimen L-RC-25x indicates that some problem occurred with the strain gauge 5 and its readings were damaged. The effect of the FR concrete can be seen comparing the compressive concrete strains in the specimens L-RC-25x and L-FRC-25x at the peak load; 2,843με and 3,038με respectively. Apparently, the specimen with FR concrete (L-FRC-25x, Fig. 17(c)) has more strain capacity than the specimen with ordinary reinforced concrete (L-RC-25x, Fig. 17(d)). Therefore, fiber reinforcement specimen presented lower deformation capacity than the other specimens.

3.4 Comparative analyses

In order to evaluate the influence of replacing the ordinary reinforcing bars by steel fibers, the values of ultimate load (P_{exp}, Table 2) are compared in Table 3. In all cases the specimens with ordinary reinforcing bars were taken as reference. For example, specimen S-FRC-0 in relation to the specimen S-RC-0, specimen S-FRC-25y compared with specimen S-RC-25y, as indicated in Table 3a. The most significant difference was recorded between the specimens L-FRC-25x and L-RC-25x which are those longer specimens with 2000 mm length and under eccentric load applied on the x axis. Furthermore, the replacement of the reinforcing bars by steel fibers reduces the effective reinforcement ratio on the cross section and this causes the lower ultimate load (see values in Table 3). According to the Table 3c, the specimens under concentric load (L-RC-0, S-RC-0, L-FRC-0 and S-FRC-0) presented lower reduction of the ultimate load than those under applied load with eccentricity e_y (L-RC-25x, S-RC-25x, L-FRC-25x and S-FRC-25x). Therefore, the slenderness ratio effect is dependent on the eccentricity of the load. Moreover, the combination of the eccentricity of the load and steel fiber (specimens L-FRC-25x and S-FRC-25x) parameters results in the most significant reduction of the ultimate load (Table 3(c)).

Table 3 Influence of investigated parameters. (a) Steel fibers, (b) Eccentricity and (c) Slenderness

(a) Fiber effect		(b) Eccentricity of load		(c) Slenderness ratio	
Specimen/ reference	P_{exp}/ P_{RF}	Specimen/ reference	P_{exp}/ P_{RE}	Specimen/ reference	P_{exp}/ P_{RS}
$\frac{S-FRC-0}{S-RC-0}$	0.91 (-8.6%)	$\frac{S-RC-25y}{S-RC-0}$	0.75 (-24.6%)	$\frac{L-RC-0}{S-RC-0}$	0.89 (-11.1%)
$\frac{S-FRC-25y}{S-RC-25y}$	0.98 (-1.8%)	$\frac{S-FRC-25y}{S-FRC-0}$	0.81 (-18.9%)	$\frac{L-FRC-0}{S-FRC-0}$	1.04 (+4.1%)
$\frac{S-FRC-25x}{S-RC-25x}$	0.99 (-0.9%)	$\frac{S-RC-25x}{S-RC-0}$	0.66 (-34.1%)	$\frac{L-RC-25x}{S-RC-25x}$	0.77 (-23.2%)
$\frac{L-FRC-0}{L-RC-0}$	1,07 (+7.0%)	$\frac{S-FRC-25x}{S-FRC-0}$	0.71 (-28.5%)	$\frac{L-FRC-25x}{S-FRC-25x}$	0.70 (-30.0%)
$\frac{L-FRC-25x}{L-RC-25x}$	0,90 (-9.8%)	$\frac{L-RC-25x}{L-RC-0}$	0.57 (-43.1%)		
		$\frac{L-FRC-25x}{L-FRC-0}$	0.48 (-52.1%)		

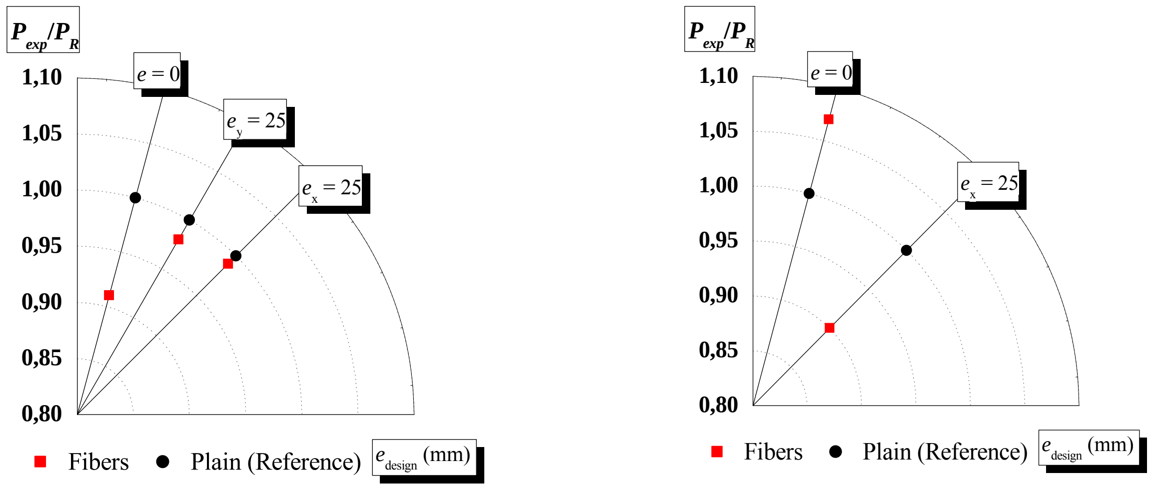

(a) Series 1 (b) Series 2

Fig. 18 Influence of the reinforcement

Specimens with ordinary reinforced concrete (L-RC-0/S-RC-0, L-RC-25x/L-RC-25x) presented reduction of the ultimate load ranged from 11.1% to 30.0% for the specimens under concentric and eccentric load respectively. Replacing the ordinary reinforced concrete by FR concrete, the longer specimen (L-FRC-0) presented higher ultimate load than the specimen with lower slenderness ratio (S-FRC-0). This behavior was unexpected and probably can been attributed to an accidental eccentricity in the specimen S-FRC-0. On the other hand, when the specimens with FR concrete under eccentric load are compared (L-FRC-25x and S-FRC-25x) , the results show that the ultimate load decreases as the slenderness ratio increases, with a ratio of 0.70 between the ultimate values (Table 3c). Therefore, as can be seen in the Table 3, a significant decrease in the ultimate load was recorded when the slenderness ratio was increased, in particular for the specimen E6 (P_{exp}=823.3 kN, in comparison to 1178.12 kN for the specimen S-FRC-25x), except to the specimen L-FRC-0.

For clarity, Figs. 18(a) and 18(b) illustrate the data of the Table 3(a), respectively for the Series 1 and 2. Using the length (L_e) to depth (b) ratio as a parameter representing these specimens this ratio was 3.95 and 13.16 for Series 1 and 2 respectively. In both, the Peak load of the specimens (P_{exp}) was taken in relation to the similar specimen with ordinary reinforced concrete (P_R). Therefore, the reference specimens were adopted as shown in Table 3. The effect of the FRC can be clearly observed in Fig. 18(a). Considering the available data in Table 3(a) and Fig. 18(a), no significant effect on the ultimate load values was observed for the Series 1 specimens due the replacement of reinforced concrete by FRC. The average load reduction was 4% and ranged from 1% (specimen S-FRC-25x in relation to S-RC-25x) to 8% (specimen S-FRC-0 in relation to S-RC-0). These comparisons indicate that there was almost no difference in the values of ultimate load for the specimens under eccentric load considering FR concrete or ordinary reinforced concrete. As mentioned before, a possible issue with the positioning of the specimen L-RC-0 caused the lower value of the ultimate load in this specimen in relation to the specimen L-FRC-0. Hence, the evaluation of the fiber effect was impaired in the longer specimens under concentric loads.

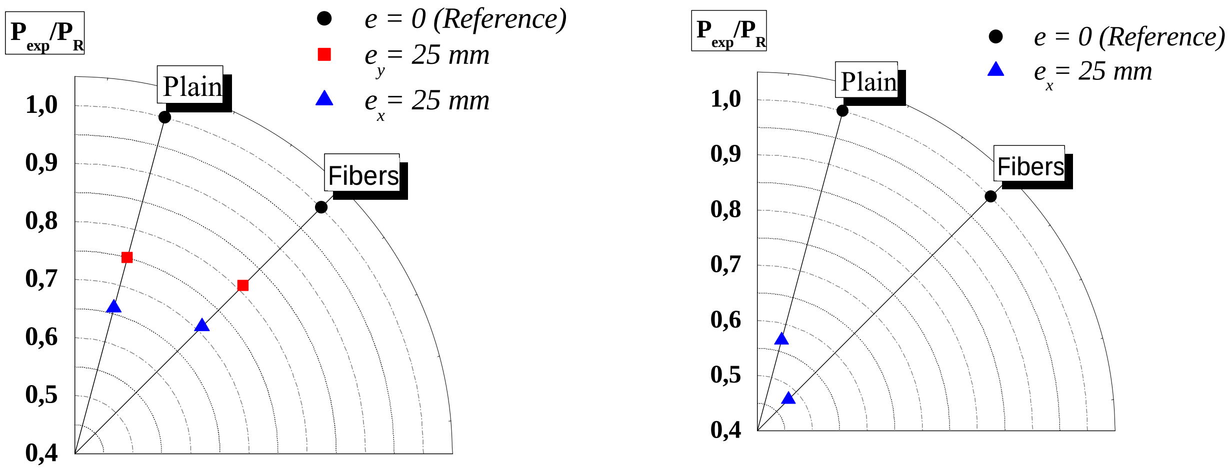

(a) Series 1 (b) Series 2

Fig. 19 Influence of load eccentricity

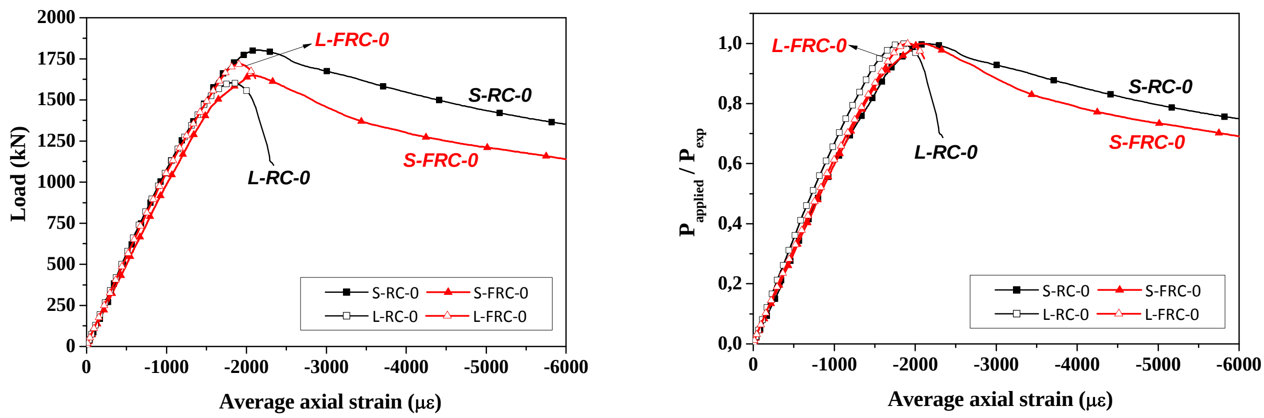

(a) (b)

Fig. 20 Load vs. average axial strain curves for concentrically loaded specimens

Similar comparison can be done considering the effect of the load eccentricity. The Peak load (P_{exp}) of specimens under concentric load was used as a reference for comparison with other specimens under eccentric load (see Table 3(b)). As shown in Table 3(b) and Fig. 19(a), the eccentricity effects were more significant when the load was applied in the x axis (eccentricity ex): reduction of 34% and 29% for specimens with ordinary reinforced concrete and with FR concrete, respectively. Regarding the specimens with applied load in the y axis, they were observed differences of 25% and 19%. These percentage reductions reveal that the ultimate load is less sensitive to the eccentricities in the y axis than in the x axis. Due to the ultimate load being more sensitive to eccentricities in the x axis, the specimens of Series 2 were only submitted to the x axis bending.

Increasing the length of the specimens magnified the eccentricity effect. Consequently, the ultimate load was reduced by 43% and 52%, for specimens with reinforced concrete or FR concrete (Fig. 19(b)), respectively. For both cases, the ultimate load values of the similar specimens under concentric load were taken as reference.

The response of all tested specimens under concentric load is shown in Fig. 20. The responses indicate that the stiffness has almost no dependence on the slenderness ratio of the columns. The non-dimensional load *vs.* Axial strains curves (Fig. 20) confirm this indicating almost the same response of all specimens until the Peak load. Unlike the pre-peak branch, the post-peak was highly influenced by the slenderness ratio and the more slender specimens (L-RC-0 and L-FRC-0) exhibited an abrupt load decrease after the peak. Among all specimens under concentric load, the specimen with FR concrete (L-FRC-0) presented no post peak branch (Fig. 20). In accordance with the Fig. 20, to the specimens S-FRC-0 and L-FRC-0 the recorded strains at the peak load were 2097με and 1919με, respectively while the specimens with ordinary reinforced concrete (S-RC-0 and L-RC-0) presented 2139με and 1832με. This comparison confirms that the longer length specimens (L-RC-0 and L-FRC-0) were less deformable than the shorter length ones.

Eccentrically loaded specimens (S-RC-25x, S-FRC-2 5x, L-RC-25x and L-FRC-25x) were more sensitive to the influence of the slenderness ratio on the ultimate l oad and axial strains response (Fig 21). Larger strains

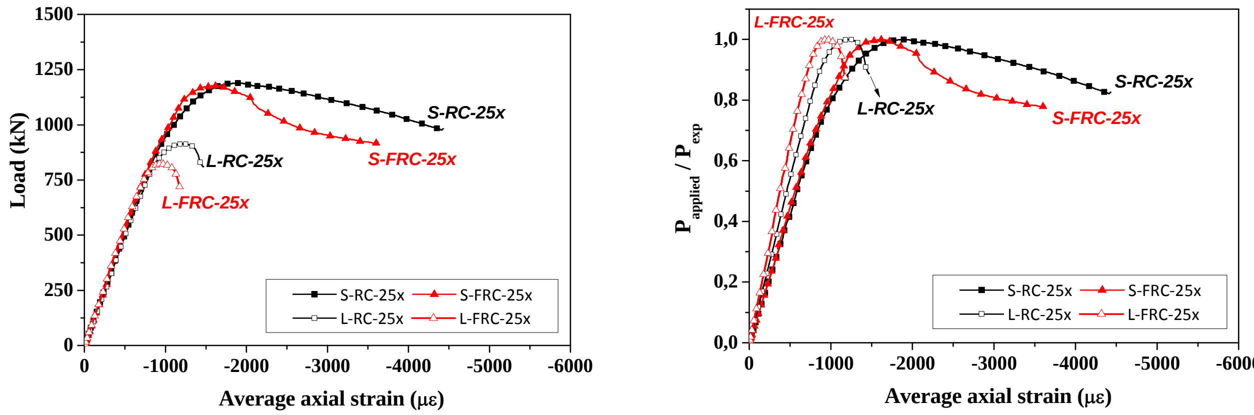

(a) (b)

Fig. 21 Influence of the slenderness ratio on specimens with eccentricity about x axis

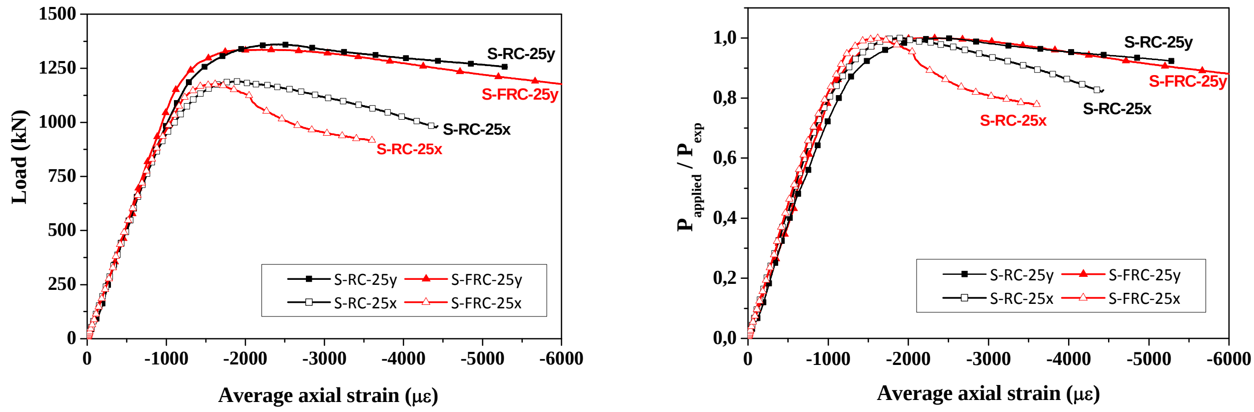

(a) (b)

Fig. 22 Influence of the eccentricity axes

were measured in the specimens with 600mm length: 1,906 and 1637 με (microstrain) for the specimens S-RC-25x and S-FRC-25x against 1,220 and 946με for the longer specimens (L-RC-25x and L-FRC-25x, respectively). Specimens with eccentric load applied in the x axis behaved differently showing that the slenderness ratio changes the post-peak branch behavior; abrupt drops and almost no residual load capacity were exhibited by the longer specimens (Fig. 21).

The eccentricity axes of loading was varied in specimens of Series 1; specimens S-RC-25y and S-FRC-25y were loaded with eccentricity in the y axis (strong-axis bending) while in the specimens S-RC-25x and S-FRC-25x the load was applied in the x axis (weak-axis bending). The influence of the eccentricity axes of loading can be observed in the Fig. 22. For bending in the strong -axis (S-RC-25y and S-FRC-25y) the specimens behaved very similarly in all stages of loading, including the post-peak branch, and presented a high residual capacity whereas for the weak-axis bending (S-RC-25x and S-FRC-25x) lower residual capacity was recorded.

5. Conclusions

This paper presented the experimental results of ten specimens of partially encased composite columns subjected to concentric and eccentric axial loading. The main goal was to investigate the effectiveness of replacing the ordinary reinforced concrete by fiber reinforced (FR) concrete. To achieve this, specimens with ordinary reinforced concrete were used as reference and submitted to the same load conditions that the specimens with FR concrete. The results obtained from the tests on short and slender composite columns allow the following conclusions to be drawn:

- The use of FR concrete has resulted in behavior and values of ultimate load very similar to those recorded by the specimens with ordinary reinforced concrete;
- The slenderness ratio has a remarkable effect on the ultimate load and behavior of the specimens mainly for composite columns under eccentric loading. The post-peak behavior was greatly affected by the slenderness ratio. Abrupt drop of load was recorded in the longer specimens while shorter specimens exhibited a more

ductile and progressive failure as well as a higher post peak residual capacity;

- All tested specimens failed by crushing of the concrete in combination with yielding of the steel. Series 1 specimens under concentric loading presented local buckling of the steel profile flanges after the peak load while the slender specimens experienced no local buckling.
- The effect of the bending axis was evaluated for the shorter specimens. The tests indicated an adverse effect on the ultimate load and post peak response of the eccentricity in the weak axis, resulting in lower residual capacity for those specimens.
- The more significant effect of the fiber reinforcement was reduce the residual capacity of the tested specimens. The deformation capacity was similar for both, FR concrete and conventional concrete specimens
- The structural capacity of the FR concrete specimens is comparable to that of the specimens with ordinary reinforced concrete. Thus, FRC can be used for the PEC columns without using reinforcing bar. However, further studies need to be performed to confirm these results.

Acknowledgments

The authors would like to acknowledge the financial support by grant #2014/12694-0 Sao Paulo State Research Support Foundation (FAPESP).

References

Altoubat, S., Ousmane, H. and Barakat, S. (2015), "Effect of fibers and welded-wire reinforcements on the diaphragm behavior of composite deck slabs", *Steel Compos. Struct.*, **19**(1), 153-171. http://dx.doi.org/10.12989/scs.2015.19.1.153.

ASTM A370 (2005), Standard Test Methods and Definitions for Mechanical Testing of Steel Products, American Society for Testing and Materials, 2005.

ABNT NBR 8800 (2008), Design and execution of steel concrete composite building structures – Procedures, Brazilian Association of Technical Codes; Rio de Janeiro, Brazil. [in Portuguese].

Begum, M., Driver, R.G. and Elwi A.E. (2013), "Behaviour of partially encased composite columns with high strength concrete", *Eng. Struct.*, **56**, 1718-1727. https://doi.org/10.1016/j.engstruct.2013.07.040.

Begum, M., Driver, R.G. and Elwi, A.E. (2015). "Parametric study on eccentrically-loaded partially encased composite columns under major axis bending", *Steel Compos. Struct.*, **19**(5), 1299-1319. http://dx.doi.org/10.12989/scs.2015.19.5.1299.

Chen, Y., Wang, T., Yang, J. and Zhao, X. (2010). "Test and numerical simulation of partially encased composite columns subject to axial and cyclic horizontal loads", *In. J. Steel Struct*, **10**(4), 385-393. https://doi.org/10.1007/BF03215846.

Chicoine, T., Tremblay, R., Massicotte, B., Ricles, J.M. and Lu, L.W. (2002), "Behavior and strength of partially encased composite columns with built-up shapes", *J. Struct. Eng.*, **128** (3), 279-288. https://doi.org/10.1061/(ASCE)0733-9445(2002)128:3(279).

Chicoine, T., Massicotte, B. and Tremblay, R. (2003), "Long-term behavior and strength of partially encased composite columns made with built-up steel shapes", *J. Struct. Eng.*, **129**(2), 141-150. https://doi.org/10.1061/(ASCE)0733-9445(2003)129:2(141).

Ellobody, E. and Ghazy, M. (2013). "Experimental investigation of eccentrically loaded fibre reinforced concrete-filled stainless steel tubular columns", *J. Constr. Steel Res.*, **76**, 167-176. https://doi.org/10.1016/j.jcsr.2012.04.001.

Ellobody, E., Alfazari, S., Alghafri, W. and Aladawi, A. (2018). "Eccentrically loaded SFRC-filled stainless steel columns", *Proc. Inst. Civ. Eng. Struct. Build.*, **1**, 1-10. https://doi.org/10.1680/jstbu.17.00165.

Ellobody, E., Alfazari, S., Alghafri, W. and Aladawi, A. (2019). "Design and testing of stainless-steel columns filled with steel-fibre reinforced concrete", *Proc. Inst. Civ. Eng. Struct. Build.*, **1**, 1-12. https://doi.org/10.1680/jstbu.18.00165.

Ebadi Jamkhaneh, M. and Kafi, M.A. (2017), "Experimental and numerical investigation of octagonal partially encased composite columns subject to axial and torsion moment loading", *Civil Eng. J.*, **3**(10), 939-955.

Eurocode 4 (2004), Design of composite steel and concrete structures – Part 1.1: General rules and rules for buildings. European Committee for standardization; Brussels, Belgium.

Gramblička, S. and Hrusovska, A. (2016), "Slenderness influence on the behavior of composite columns", *Key Eng. Mater.*, **691**, 40-50. https://doi.org/10.4028/www.scientific.net/KEM.691.40.

Gramblička, S. and Matiaski, S. (2009), "Theorical and experimental analyses on composite columns with use of high strength concrete", *Slovak J. Civil Eng.*, **4**, 31- 40.

Hatzigeorgiou, G.D. and Beskos, D.E. (2005), "Minimum cost design of fibre-reinforced concrete-filled steel tubular columns", *J. Constr. Steel Re.s*, **61**(2), 167-182. https://doi.org/10.1016/j.jcsr.2004.06.003.

Hunaiti, Y.M. and Fattah, B.A. (1994), "Design considerations of partially encased composite columns", *Proc. Inst. Civ. Eng., Struct. Build.*, **106**, 75-82. https://doi.org/10.1680/istbu.1994.25681.

Lai, B., Liew, J.Y.R. and Xiong, M. (2019), "Experimental and analytical investigation of composite columns made of high strength steel and high strength concrete", *Steel Compos. Struct.*, **33**(1), 67-79. http://dx.doi.org/10.12989/scs.2019.33.1.067.

Lu, Y., Liu, Z., Li, S. and Li, W. (2017), "Behavior of steel fibers reinforced self-stressing and self-compacting concrete-filled steel tube subjected to bending", *Constr. Build. Mater.*, **156**, 639-651. https://doi.org/10.1016/j.conbuildmat.2017.09.019.

Lu, Y., Liu, Z., Li, S. and Li, N. (2018), "Bond behavior of steel fibers reinforced self-stressing and self-compacting concrete filled steel tube columns", *Constr. Build. Mater.*, **158**, 894-909. https://doi.org/10.1016/j.conbuildmat.2017.10.085.

Oh, M.H., Ju, Y.K., Kim, M.H. and Kim, S.D. (2006), "Structural performance of steel-concrete composite column subjected to axial and flexural loading", *J. Asian Architect. Build. Eng.*, **5**(1), 153-160. https://doi.org/10.3130/jaabe.5.153.

Pereira, M.F., De Nardin, S. and El Debs, A.L.H.C. (2016), "Structural behavior of partially encased composite columns under axial loads", *Steel Compos. Struct.*, **20**(6), 1305-1322. http://dx.doi.org/10.12989/scs.2016.20.6.1305.

Prickett, B.S. and Driver, R.G. (2006), "Behavior of Partially Encased Columns Made with High Performance Concrete", Structural Engineering Report No 262; Dept. of Civil and Enviroment Eng., University of Alberta, Canada.

Song, Y.C., Wang, R.P. and Li, J. (2016), "Local and post-local buckling behavior of welded steel shapes in partially encased composite columns", *Thin-Wall. Struct*., **108**, 93-108. https://doi.org/10.1016/j.tws.2016.08.003.

Tokgoz, S. and Dundar, C. (2010), "Experimental study on steel tubular columns in-filled with plain and steel fiber reinforced concrete", *Thin-Wall. Struct*., **48**(6), 414-422. https://doi.org/10.1016/j.tws.2010.01.009.

Tokgoz, S. (2015), "Tests on plain and steel fiber concrete-filled stainless steel tubular columns", *J. Constr. Steel Res*, **114**, 129-135. https://doi.org/10.1016/j.jcsr.2015.07.013.

Tremblay, R., Chicoine, T. and Massicotte, B. (2000), "Design equation for the axial capacity of partially encased non-compact columns", *Proceedings of the Composite Construction in Steel and Concrete IV Conference 2000*, Alberta, Canada.

Vincent, R.B. (2000), "Design and application of partially encased non-compact composite columns for high-rise buildings", *Proceedings of the Composite Construction in Steel and Concrete IV Conference 2000*, Alberta, Canada.

Wang, H., Li, J. and Song, Y. (2019), "Numerical study and design recommendations of eccentrically loaded partially encased composite columns", *Int. J. Steel Struct.*, **19**(3), 991-1009. *https://doi.org/10.1007/s13296-018-0179-7.*

Wu, B., Jian, S.M. and Zhao, X.Y. (2019), "Structural behavior of steel-concrete partially encased composite columns containing demolished concrete lumps under axial compression", *Eng. Struct.*, **197**, 109383. https://doi.org/10.1016/j.engstruct.2019.109383.

CC